Title: LA-ICP-MS U-Pb dating and REE patterns of apatite from the Tatra Mountains, Poland as a monitor of the regional tectonomagmatic activity

Author: Aleksandra Gawęda, Krzysztof Szopa, David Chew

Citation style: Gawęda Aleksandra, Szopa Krzysztof, Chew David. (2014). LA-ICP-MS U-Pb dating and REE patterns of apatite from the Tatra Mountains, Poland as a monitor of the regional tectonomagmatic activity. "Geochronometria" (Vol. 41, iss. 4, (2014), s. 306-314), doi 10.2478/s13386-013-0171-0

VERSITA

GEOCHRONOMETRIA 41(4) 2014: 306–314
DOI 10.2478/s13386-013-0171-0

Available online at
www.springerlink.com

LA-ICP-MS U-Pb DATING AND REE PATTERNS OF APATITE FROM THE TATRA MOUNTAINS, POLAND AS A MONITOR OF THE REGIONAL TECTONOMAGMATIC ACTIVITY

ALEKSANDRA GAWĘDA[1], KRZYSZTOF SZOPA[1] and DAVID CHEW[2]
[1]*Faculty of Earth Sciences, University of Silesia, Bedzińska st. 60, 41-200 Sosnowiec, Poland*
[2]*Department of Geology, School of Natural Sciences, Trinity College Dublin, Dublin 2, Ireland*

Received 9 February 2014 Accepted 3 July 2014

Abstract: This study presents apatite LA-ICP-MS U-Pb age and trace elements concentrations data from different granite types from the Tatra Mountains, Poland. Apatite from monazite and xenotime-bearing High Tatra granite was dated at 339 ± 5 Ma. The apatite LREE patterns reflect two types of magmas that contributed to this layered magma series. Apatite from a hybrid allanite-bearing diorite from the Goryczkowa Unit was dated at 340 ± 4 Ma with apatite LREE depletion reflecting the role of allanite and titanite during apatite crystallization. Apatite crystals from a hybrid cumulative rock from the Western Tatra Mountains were dated at 344 ± 3 Ma. Apatite is one of the main REE carriers in this sample and exhibit flat REE patterns.
Taking into account the relatively low closure temperature of the U-Pb system in apatite (350–550°C), the *c.* 340 Ma apatite ages mark the end of high temperature tectonometamorphic activity in the Tatra Mountains.

Keywords: apatite, U-Pb age, REE patterns, Tatra Mountains.

1. INTRODUCTION

Apatite is a nearly ubiquitous accessory phase in igneous rocks due to the low solubility of P_2O_5 in silicate melts and the limited amount of phosphorus incorporated into the crystal lattices of the major rock-forming minerals (Piccoli and Candela, 2002). Apatite is an important carrier of many trace elements (Sha and Chappell, 1999), and can control the budget of Y and REE, especially in rocks with high apatite contents (Dempster *et al.*, 2003; Prowatke and Klemme, 2006; Szopa *et al.*, 2013). Recently apatite has been used in high-temperature thermochronological studies, showing that the closure temperature of the uranium — lead (U-Pb) system is approximately 350–550°C (Chamberlain and Bowring, 2000; Schoene and Bowring, 2007; Cochrane *et al.*, 2014). As the U^{+4} and Pb partition coefficients are not significantly affected by melt composition, apatite can be used as a geochronometer in a wide variety of igneous rock types. Apatite LA-ICP-MS (Laser Ablation Inductively Coupled Plasma Mass Spectrometry) U-Pb and Th-Pb ages can exhibit low weighted mean age uncertainties as low as 1–2% (Chew *et al.*, 2011). As the U-Pb closure temperature for apatite is relatively low, apatite U-Pb ages cannot be interpreted in terms of the timing of magmatic activity. However, apatite U-Pb data does yield valuable information on the timing of thermal events and the cooling histories of crystalline basement terranes.

Corresponding author: A. Gawęda
e-mail: aleksandra.gaweda@us.edu.pl

ISSN 1897-1695 (online), 1733-8387 (print)

This study investigates the utility of apatite LA-ICP-MS U-Pb dating to constrain the timing of magmatic and tectonothermal activity in the polygenetic Tatra Mountains granite suite. The age of the youngest magmatic activity in the Tatra Mountains has been debated for many years. Magmatic ages as young as 315 Ma have been suggested in the literature (Poller and Todt, 2000), but more recently the youngest magmatic activity in the High Tatra granite suite has been constrained at 337 ± 6 Ma by LA-MC-ICP-MS U-Pb zircon dating (Burda *et al.*, 2013a). We also compare apatite REE (Rare Earth Elements) and trace element (e.g. Y, Sr) concentration data relative to the parent rocks samples to monitor the role of apatite as a carrier-phase for these elements.

Three granite types were sampled in this study, including: the High Tatra syenogranite (HTG), the Goryczkowa diorite-granodiorite (GDG) and an apatite-rich cumulate from the hybrid Western Tatra granitoid (WTC; **Fig. 1b**). All three samples have yielded different LA-ICP-MS U-Pb zircon ages (337 ± 6 Ma, 371 ± 6 Ma and 368 ± 8 Ma adequately) and represented genetically different magmatic pulses within a polygenetic layered intrusion (Burda *et al.*, 2013a, 2013b; 2011).

2. GEOLOGICAL SETTING AND SAMPLING

The crystalline core of the Tatra mountains comprises a Variscan polygenetic granitoid pluton and its metamorphic envelope (**Fig. 1b**; Morozewicz, 1914; Kohut and Janak, 1994; Gawęda, 2009), that is partly covered by Mesozoic sedimentary rocks. The metamorphic envelope to the polygenetic granitoid intrusion is exposed in the western part of the massif and is strongly migmatised (Burda and Gawęda, 2009; **Fig. 1b**). The tabular granitoid pluton is composed of several magma batches, that differ in age and chemistry. In the Western Tatra Mountains (**Fig. 1b**) an Early-Variscan hybridization episode is represented by I-type quartz-diorite hybrid precursors (368 ± 8 Ma by the U-Pb method on zircon; Gawęda *et al.*, 2005; Burda *et al.*, 2011), which occur as sills within the metamorphic envelope and at the base of the granodiorite-tonalite intrusion (360–345 Ma; Poller *et al.*, 2000). A suite of unusual apatite-rich rocks of cumulative origin is linked to this hybridization episode (Szopa *et al.*, 2013). In the eastern part of the crystalline core (High Tatra Mountains) syenogranite-monzogranite is most abundant, locally with mafic microgranular enclaves

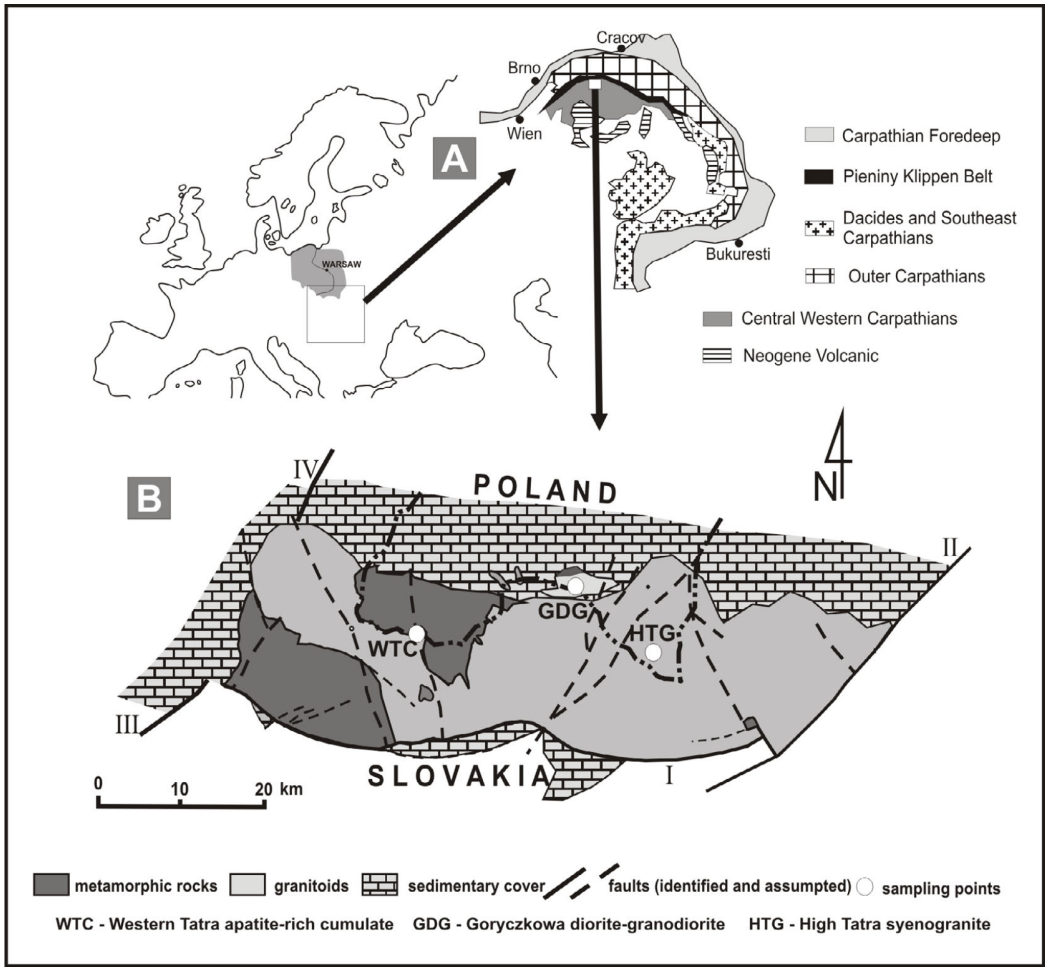

Fig. 1. *The position of the Tatra Mountains in the Carpathian Chain (a) and a simplified geological map with the location of sampling points (b).*

(MME) and metasedimentary xenoliths (Gawęda, 2009 and references therein). These granitoids exhibit characteristic magmatic layering (Gawęda and Szopa, 2011) and were emplaced between 361–337 Ma (Gawęda, 2008; Burda *et al.*, 2013a). The Goryczkowa granite, which crops out in the crystalline cores of the Alpine nappes (Jurewicz 2006; **Fig. 1b**), is comprised of granodiorite-diorite, and was dated at *c.* 371 Ma and was followed by the intrusion of K-feldspar–rich leucogranite dated at *c.* 350 Ma by the LA-ICPMS U-Pb method on zircons (Burda *et al.*, 2013b).

All these granitoid pulses show geochemical and isotopic signatures suggesting that the granitoid melts were produced by melting of a heterogeneous package of metasedimentary rocks during subduction of oceanic crust under the continental wedge and interaction with mantle derived melts (Broska and Uher, 2001; Gawęda, 2009; Burda *et al.*, 2011, 2013a, 2013b).

Post-magmatic extension and associated shearing resulted in the formation of localized shear zones and metamorphic fabrics in the magmatic rocks, resulted in $^{40}Ar/^{39}Ar$ biotite ages of c. 322–331 Ma interval (Kohut and Sherlock, 2003).

3. ANALYTICAL METHODS

Petrography

For this study we used magmatic rock samples, that were previously dated by the LA-MC-ICP-MS zircon U-Pb method (Burda *et al.*, 2011, 2013a, 2013b) and one sample of an apatite-rich cumulate (Szopa *et al.*, 2013). Petrographical analyses of thin sections were undertaken to check the apatite content and its morphological varieties. These observations formed the basis for selecting samples for the subsequent isotopic analyses.

Apatite morphology, chemistry and U-Pb dating

Apatite crystals were separated using standard techniques (crushing, hydrofracturing, washing, Wilfley shaking table, Frantz magnetic separator and handpicking). The separation was carried out at the Institute of Geological Sciences, Polish Academy of Sciences, Cracow. The samples were then mounted in 25 mm diameter epoxy resin pucks, then grinded and polished to expose the grain interiors. The apatite crystal morphologies were imaged by scanning electron microscopy on a FET Philips 30 electron microscope (15 kV and 1 nA) at the Faculty of Earth Sciences, University of Silesia, Sosnowiec, Poland.

For trace element and isotopic analyses only unzoned apatite crystals were selected from all three granitoid samples. Apatite U-Pb data were acquired using a Photon Machines Analyte Exite 193 nm ArF Excimer laser-ablation system coupled to a Thermo Scientific iCAP Qc at the Department of Geology Trinity College Dublin. Twenty eight isotopes (^{31}P, ^{35}Cl, ^{43}Ca, ^{55}Mn, ^{86}Sr, ^{89}Y, ^{139}La, ^{140}Ce, ^{141}Pr, ^{146}Nd, ^{147}Sm, ^{153}Eu, ^{157}Gd, ^{159}Tb, ^{163}Dy, ^{165}Ho, ^{166}Er, ^{169}Tm, ^{172}Yb, ^{175}Lu, ^{200}Hg, ^{204}Pb, ^{206}Pb, ^{207}Pb, ^{208}Pb, ^{232}Th, ^{238}U and mass 248($^{232}Th^{16}O$) were acquired using a 50 µm laser spot, a 4 Hz laser repetition rate and a fluence of 3.31 J/cm^2. A *c.* 1 cm sized crystal of Madagascar apatite which has yielded a weighted average ID-TIMS concordia age of 473.5 ± 0.7 Ma (Cochrane *et al.*, 2014) was used as the primary apatite reference material in this study. McClure Mountain syenite apatite was used as a secondary standard. McClure Mountain syenite has moderate but reasonably consistent U and Th contents (~23 ppm and 71 ppm, Chew and Donelick, 2012) and its thermal history, crystallization age (weighted mean $^{207}Pb/^{235}U$ age of 523.51 ± 2.09 Ma) and initial Pb isotopic composition ($^{206}Pb/^{204}Pb$ = 17.54 ± 0.24; $^{207}Pb/^{204}Pb$ = 15.47 ± 0.04) are known from high-precision TIMS analyses (Schoene and Bowring, 2006). NIST 612 standard glass was used as the apatite trace element concentration reference material.

The raw isotope data were reduced using the "Vizual Age" data reduction scheme (Petrus and Kamber, 2012) of the freeware IOLITE package of Paton *et al.* (2011). User-defined time intervals are established for the baseline correction procedure to calculate session-wide baseline-corrected values for each isotope. The time-resolved fractionation response of individual standard analyses is then characterised using a user-specified down-hole correction model (such as an exponential curve, a linear fit or a smoothed cubic spline). The data reduction scheme then fits this appropriate session-wide "model" U-Th-Pb fractionation curve to the time-resolved standard data and the unknowns. Sample-standard bracketing is applied after the correction of down-hole fractionation to account for long-term drift in isotopic or elemental ratios by normalizing all ratios to those of the U-Pb reference standards. Common Pb in the primary apatite standard was corrected using the ^{207}Pb-based correction method using a modified version of the VizualAge DRS (Chew *et al.*, 2014). Over the course of two months of analyses, the McClure Mountain apatite secondary standard ($^{207}Pb/^{235}U$ TIMS age of 523.51 ± 1.47 Ma; Schoene and Bowring, 2006) yielded a U-Pb Tera-Wasserburg concordia lower intercept age of 524.5 ± 3.7 Ma with an MSWD = 0.72. The regression line was anchored to lower intercept using a $^{207}Pb/^{206}Pb$ value of 0.88198, derived from an apatite ID-TIMS total U-Pb isochron (Schoene and Bowring, 2006). REE contents were normalized to C1 chondrite (Sun and McDonough, 1989).

4. RESULTS

Petrography and whole-rock chemistry

Three types of peraluminous granitoids, all showing features characteristic of magma mixing, were investigated:

1) Strongly layered High Tatra — type that is represented by coarse-grained biotite granodiorite (**Fig.**

2a), dated at 345 ± 6 Ma to 337 ± 6 Ma by LA-MC-ICP-MS U-Pb zircon dating (Burda *et al.*, 2013a). Accessory minerals are represented by zircon, apatite and monazite. The chondrite-normalized REE diagram reveals moderate to high REE fractionation with Ce_N/Yb_N = 18.2–32.4 and a weak to pronounced negative Eu anomaly (Eu/Eu* = 0.9–0.5; Burda *et al.*, 2013a; **Fig. 3a**).

2) Porphyritic to equigranular medium-grained Goryczkowa-type diorite — granodiorite (**Fig. 2b**) that was dated at 371 ± 6 Ma (Burda *et al.*, 2013b). Accessory minerals are represented by zircon, apatite, zoned allanite and titanite. The REEs show moderate fractionation (Ce_N/Yb_N = 20.8–24.2) and a weakly negative to slightly positive Eu anomaly (Eu/Eu* = 0.8–1.0; Burda *et al.*, 2013b; **Fig. 3b**).
3) Apatite-rich cumulate rock, composed of feldspar, apatite, quartz and biotite. Magmatic zircon is absent although idiomorphic, zoned monazite is present in small quantities. As these rocks have demonstrated to be genetically linked to the mixing and mingling of two different magmas, the zircon U-Pb age of the mingled hybrid (368 ± 8 Ma; Burda *et al.*, 2011) is considered to constrain the age of these rocks. Apatite-rich cumulates show low degree of REE fractionation and negative Eu anomalies (Eu/Eu* = 0.4–0.7; Szopa *et al.*, 2013; **Fig. 3c**).

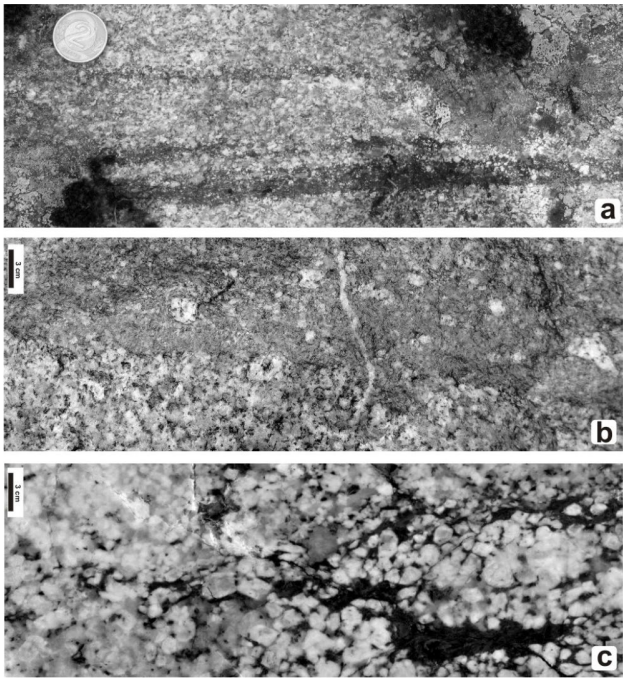

Fig. 2. *Three petrographical types of the Tatra granitoids: layered High Tatra granite (a), granodiorite-diorite Goryczkowa type (b) and Western Tatra apatite-rich cumulate (c).*

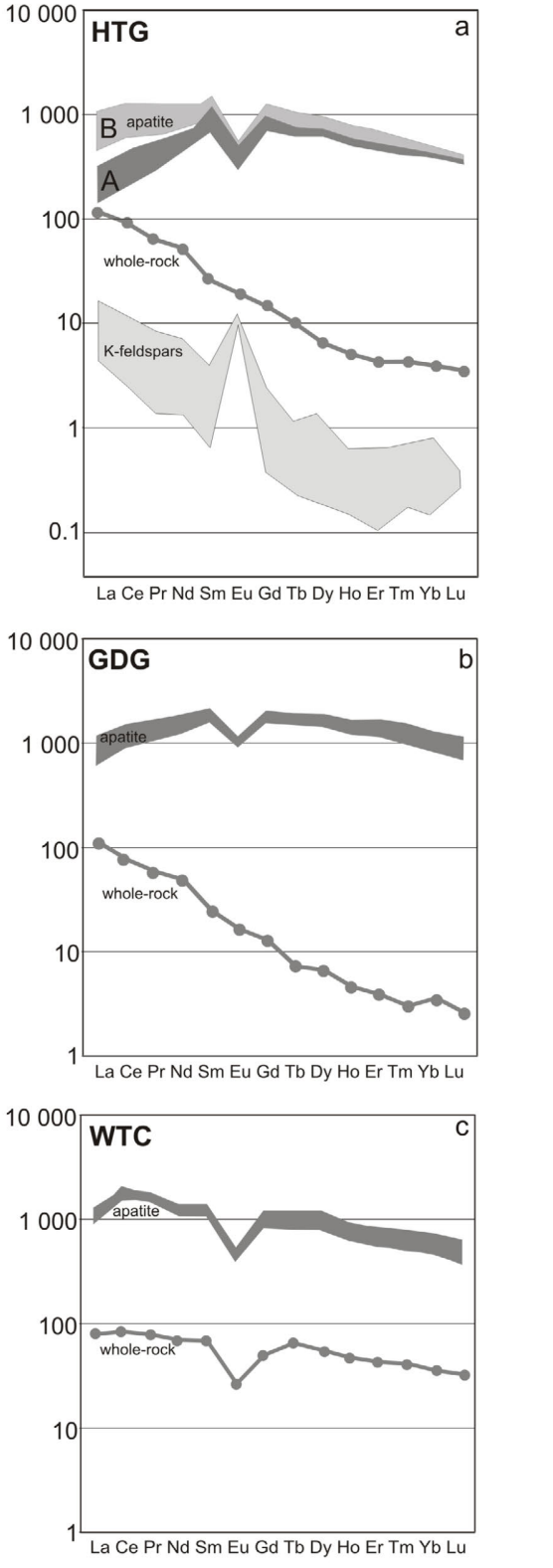

Fig. 3. *Chondrite (C1)-normalized REE patterns of apatites from three types of the Tatra granitoids (rock data for comparison are from Burda* et al.*, 2013a, 2013b and Szopa* et al.*, 2013). K-feldspar REE patterns (raw data from Gawęda and Sikorska, 2009 database) are used for comparison in (a)*

Apatite characteristics

The ap atite crystals from the all granite samples can be classified as apatite-(Ca,F) with 2.9–3.7 wt% of F (*ca.* 1.8 atoms per 2 (OH, F, Cl)).

In the layered High Tatra granite (HTG) both zoned and homogeneous apatite crystals are 0.1 to 0.8 mm long and 0.1–0.2 mm wide; in general stubby apatite dominates over the more prismatic varieties (**Figs. 4a** and **4b**). Sr contents range from 549 to 562 ppm (mean value 583 ppm), Y ranges from 1005 to 1551 ppm (mean value 1367 ppm) and Mn content ranges from 647to 1557 ppm (**Table 1**). Zoned crystals are relatively rare and are found only in mafic microgranular enclaves (Gawęda, 2009) and chemical zonation, where present, is defined by variations in the Y content, and typically is higher in the cores compared to the rims (**Fig. 4c**). Chondrite (C1)-normalized REE patterns of apatite are dominated by very weak REE fractionation (La_N/Yb_N = 0.66–1.04), negative Eu anomalies (0.39–0.44) and slightly positive Ce anomalies (Ce/Ce* ~1.1; **Table 1**, **Fig. 3a**). Two types of LREE fractionation patterns could be distinguished here: HTG-A with a steep La-Sm depletion (La/Sm = 0.2–0.4) and associated with the lowest Y contents and HTG-B, with almost flat LREE patterns (La_N/Sm_N = 0.5–0.8). HREE patterns are relatively consistent throughout the analysed grains and are characterised by Gd/Lu ratios in the range of 2.4–3.2 (**Table 1**, **Fig. 3a**).

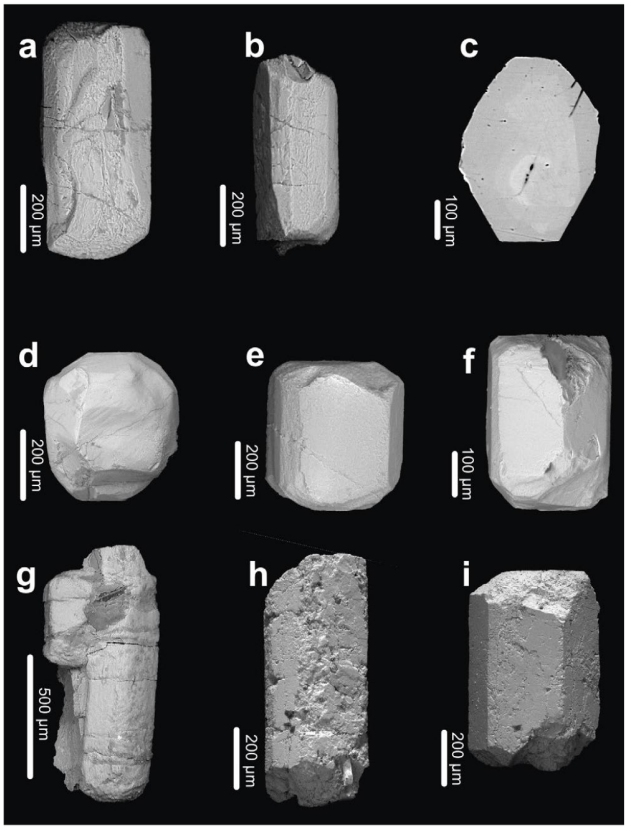

Fig. 4. *Apatite morphology and CL (c) characteristic from three types of granitoids: HTG (a–c), GDG (d–f) and WTC (g–i).*

Equant apatite-(Ca, F) crystals from hybrid Goryczkowa-type diorite are 0.1 to 0.6 mm long and up to 0.7 mm wide (**Figs. 4d** and **4e**). No zonation was noted (**Fig. 4f**). Analysed crystals show moderate and relatively consistent Sr contents (616–784 ppm; mean value 692 ppm), Y contents (1542–2455 ppm; mean value 2150 ppm) and variable Mn concentrations (974–2987 ppm; **Table 1**). REE patterns are characterized by very weak fractionation, dominated by HREE enrichment (La_N/Yb_N = 0.5–2.4; La_N/Sm_N = 0.2–0.8), small positive Ce anomaly (Ce/Ce* = 1.0–1.1) and a strongly negative Eu anomaly (Eu/Eu* = 0.3–0.4; **Fig. 3b**; **Table 1**).

In the apatite-bearing cumulate rock from the Western Tatra Mountains, apatite-(Ca, F) is one of the main rock-forming minerals. Long-prismatic, idiomorphic crystals, 0.1–0.7 mm in length, with elongation ratios ranging from 4:1 to 8:1, represent the most common morphological type (**Figs. 4f** and **4g**). They are usually unzoned (**Fig. 4h**) and sporadically reveal internal zoning caused by Fe, Mn, Mg and Y substitutions (Szopa *et al.*, 2013). The analyzed crystals show Sr contents of 287–457 ppm (mean value 397 ppm), 870–1300 ppm Y (mean value 1123 ppm) and strongly variable Mn contents (1394–3950 ppm). Low REE fractionation with typical HREE depletion (La_N/Yb_N = 1.4–2.4) and a weakly negative slope for the LREE (La/Sm = 0.7–1.0) with a distinct positive Ce anomaly (Ce/Ce* = 1.2–1.7) and negative Eu anomaly (Eu/Eu* = 0.4–0.5; **Table 1**) are characteristic features of the chondrite-normalized apatite REE patterns (**Fig. 3c**).

Apatite dating

U-Pb apatite data from three samples from the Tatra Massif: a layered High Tatra granite (HTG), hybrid Goryczkowa-type diorite (GTG) and an apatite-bearing cumulative rock from the Western Tatra Mountains (WTC) lie on the discordias as a result of variable incorporation of common Pb. The samples yield Tera Wasserburg lower intercept ages of 339.5 ± 4.4 Ma (MSDW = 1.8), 338.8 ± 5.3 Ma (MSDW = 1.6) and 344.3 ± 2.8 Ma (MSDW = 4.8) respectively (**Figs. 5a**, **5b** and **5c**; **Table 2**). The discordias were anchored using the Stacey and Kramers (1975) terrestial Pb evolution model calculated for the apatite U-Pb age of each sample. Taking into account the age uncertainties, the U-Pb data could be assumed to group around 340 Ma, which is consistent (within uncertainty) of the youngest U-Pb zircon age of 337 ± 6 Ma (Burda *et al.*, 2013a).

Table 1. *Representative apatite LA-ICP-MS analyses of REE, Y and Mn, with calculated petrological indices: Eu/Eu* = Eu/√Sm·Gd; Ce/Ce* = Ce/√ La·Pr. Normalization of La, Sm, Yb was calibrated after Sun and McDonough (1989).*

	Apatite from the monazite-bearing High Tatra granite (HTG)						Apatite from diorite (GDG)						Apatite from the Western Tatra Mts cumulate (WTC)						*LOD*
La (ppm)	772	777	845	899.45	949	694	565	556	818	721	941	902	821	925	978	894	834	973	65.00
Ce	1250	1205	1197	1258	1354	1102	830	882	1107	1103	1255	1218	1586	1617	1590	1518	1448	1441	98.00
Pr	1538	1468	1379	1442	1553	1342	1057	1144	1309	1381	1475	1431	1428	1435	1490	1418	1372	1451	7.60
Nd	1805	1737	1561	1640	1795	1567	1412	1465	1589	1726	1775	1733	1064	1095	1103	997	1013	1051	34.00
Sm	2192	2186	1977	2039	2239	2054	1667	1801	1802	1975	2012	1953	1132	1091	1136	1031	1086	1007	4.20
Eu	800	819	836	865	929	831	574	620	624	630	727	698	399	397	413	385	382	395	0.48
Gd	1880	1992	1851	1912	2084	1948	1510	1579	1530	1647	1730	1659	941	838	899	833	851	809	3.80
Tb	1632	1766	1706	1769	1897	1800	1223	1323	1251	1334	1408	1343	934	855	838	823	815	774	0.50
Dy	1518	1729	1696	1746	1882	1773	1131	1227	1161	1241	1295	1252	947	838	837	827	809	721	3.01
Ho	1203	1401	1444	1500	1574	1475	911	995	934	1006	1056	1006	750	643	671	633	638	571	0.55
Er	1160	1381	1459	1515	1582	1466	817	899	838	904	938	891	647	608	571	533	586	530	1.60
Tm	956	1164	1254	1308	1365	1246	673	756	693	748	781	745	616	557	558	499	560	489	0.25
Yb	742	913	1023	1076	1082	996	569	638	582	636	658	622	572	554	519	446	523	463	1.01
Lu	611	763	865	927	929	837	474	534	481	539	545	520	472	443	417	363	436	382	0.16
Y	1542	2290	1880	2190	2261	2318	1338	1457	1369	1467	1551	1478	967	1160	1202	983	1068	1061	0.32
Mn	974	2987	2035	2076	2809	2987	1180	647	1246	701	1557	1542	648	837	1031	1428	930	872	18.00
(La/Yb)N	1.04	0.85	0.83	0.84	0.88	0.70	0.99	0.87	1.41	1.13	1.43	1.45	1.44	1.67	1.88	2.00	1.60	2.10	
(La/Sm)N	0.35	0.36	0.43	0.44	0.42	0.34	0.34	0.31	0.45	0.37	0.47	0.46	0.73	0.85	0.86	0.87	0.77	0.97	
Ce/Ce*	1.15	1.13	1.11	1.10	1.12	1.14	1.07	1.11	1.07	1.11	1.07	1.07	1.46	1.40	1.32	1.35	1.35	1.21	
Eu/Eu*	0.39	0.39	0.44	0.44	0.43	0.42	0.36	0.37	0.38	0.35	0.39	0.39	0.39	0.41	0.41	0.42	0.40	0.44	

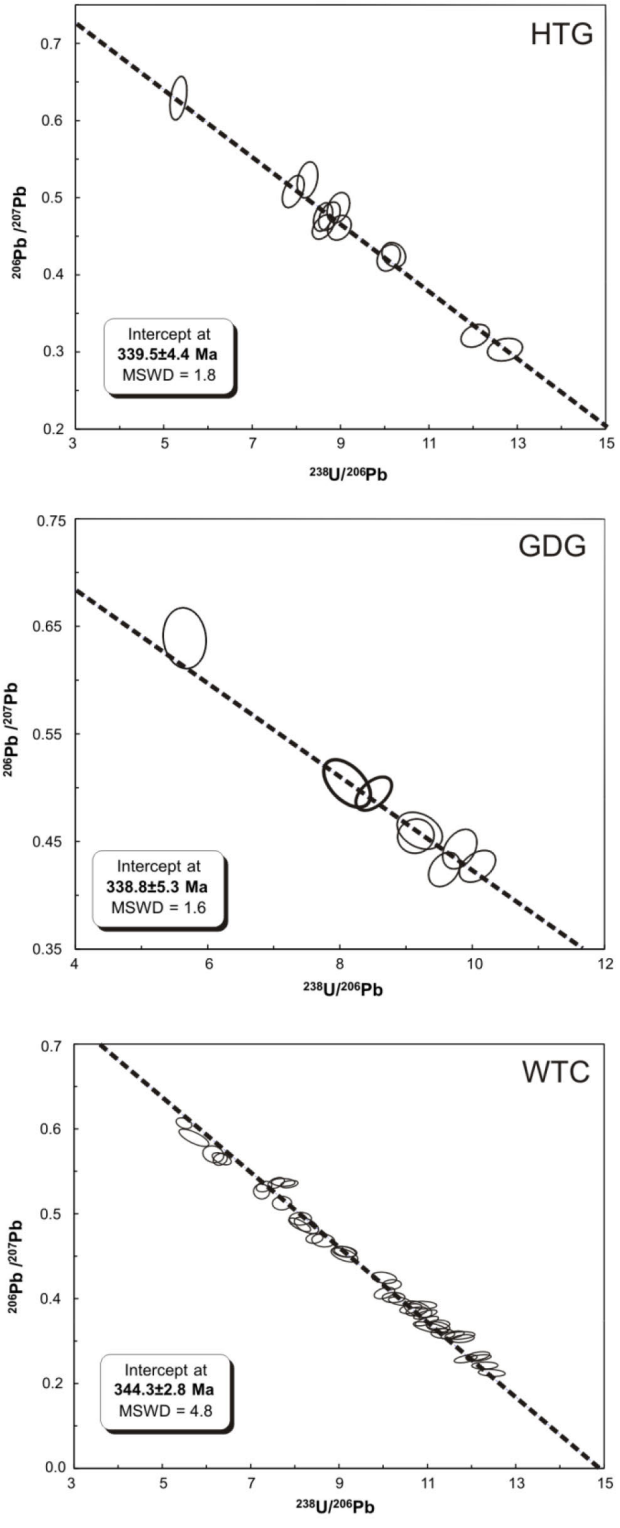

Fig. 5. *Tera-Wasserburg concordia diagrams anchored through common Pb for HTG (a), GDG (b) and WTC (c).*

Table 2. *Apatite isotopic age data from three granitoid types.*

Locality		$^{207}Pb/^{235}U$	±2σ	$^{206}Pb/^{238}U$	±2σ	ρ	$^{238}U/^{206}Pb$	±2σ	$^{207}Pb/^{206}Pb$	±2σ	ρ	$^{206}Pb/^{238}U$ age	±2σ Ma	$^{207}Pb/^{235}U$ age	±2 σ Ma	$^{207}Pb/^{206}Pb$ age	±2σ Ma	^{207}Pb corr. age	±2σ Ma
GDG	1	15.43	0.95	0.177	0.008	0.79	5.653	0.265	0.639	0.023	-0.08	1050.0	49.3	2842.2	175.0	4599.3	165.5	302.4	35.4
	2	8.42	0.48	0.123	0.004	0.93	8.110	0.289	0.504	0.018	-0.50	749.5	26.7	2277.3	129.8	4253.0	151.9	340.3	21.3
	3	8.31	0.27	0.120	0.002	0.15	8.327	0.173	0.496	0.015	0.34	731.1	15.2	2265.4	73.6	4229.4	127.9	339.0	16.1
	4	6.99	0.28	0.109	0.003	0.56	9.149	0.226	0.455	0.013	0.05	668.7	16.5	2110.2	84.5	4101.6	117.2	343.4	14.2
	5	6.03	0.21	0.104	0.002	0.17	9.578	0.193	0.424	0.013	0.31	640.1	12.9	1980.2	69.0	3996.4	122.5	353.1	12.9
	6	5.86	0.17	0.099	0.002	0.23	10.081	0.224	0.427	0.012	0.39	609.7	13.5	1955.3	56.7	4007.0	112.6	333.5	12.1
	7	6.84	0.32	0.109	0.003	0.86	9.208	0.280	0.46	0.014	-0.32	664.6	20.2	2090.9	97.8	4117.9	125.3	337.1	15.8
	8	6.23	0.22	0.102	0.002	0.17	9.813	0.212	0.443	0.015	0.34	625.5	13.5	2008.7	70.9	4061.9	137.5	329.9	14.1
HTG	1	7.40	0.22	0.116	0.003	0.30	8.606	0.200	0.462	0.013	0.41	708.7	16.5	2161.0	64.2	4124.3	116.1	358.5	14.7
	2	3.29	0.13	0.079	0.002	0.26	12.723	0.324	0.303	0.012	0.21	487.8	12.4	1478.7	58.4	3485.6	138.0	340.2	11.3
	3	5.79	0.22	0.098	0.002	0.74	10.204	0.219	0.426	0.013	-0.18	602.7	12.9	1944.9	73.9	4003.5	122.2	330.3	12.4
	4	3.64	0.14	0.083	0.002	0.07	12.048	0.261	0.321	0.012	0.29	514.0	11.1	1558.3	59.9	3574.6	133.6	347.5	10.8
	5	7.14	0.26	0.111	0.003	0.38	8.977	0.218	0.461	0.013	0.25	680.9	16.5	2129.0	77.5	4121.1	116.2	344.8	14.3
	6	7.45	0.24	0.114	0.003	0.14	8.749	0.199	0.476	0.015	0.40	697.7	15.9	2167.0	69.8	4168.6	131.4	340.4	15.7
	7	7.54	0.28	0.112	0.003	0.19	8.952	0.208	0.487	0.016	0.30	682.6	15.9	2177.8	80.9	4202.3	138.1	323.4	16.1
	8	8.90	0.32	0.126	0.003	0.07	7.930	0.201	0.508	0.017	0.45	765.6	19.4	2327.8	83.7	4264.6	142.7	344.0	19.1
	9	5.80	0.21	0.099	0.002	0.24	10.091	0.214	0.422	0.014	0.24	609.1	12.9	1946.4	70.5	3989.4	132.3	337.0	13.1
	10	8.75	0.34	0.121	0.003	0.27	8.251	0.191	0.523	0.019	0.26	737.5	17.0	2312.3	89.8	4307.4	156.5	316.9	19.7
	11	16.36	0.68	0.188	0.005	0.52	5.330	0.156	0.629	0.023	0.34	1108.4	32.5	2898.1	120.5	4576.5	167.3	334.8	35.6
	12	7.58	0.24	0.116	0.002	0.07	8.606	0.178	0.475	0.015	0.32	708.7	14.6	2182.5	69.1	4165.4	131.5	346.9	15.6
WTC	1	99.90	5.00	0.842	0.035	0.73	1.188	0.049	0.862	0.031	0.23	3937.8	163.7	4685.1	234.5	5027.8	180.8	-166.0	224.7
	2	46.50	3.20	0.368	0.002	0.59	2.717	0.148	0.925	0.049	0.23	2020.0	109.8	3920.1	269.8	5127.6	271.6	-264.4	154.6
	3	196.00	11.00	1.652	0.091	0.90	0.605	0.033	0.866	0.023	0.19	6287.3	346.3	5364.5	301.1	5034.4	133.7	-384.7	346.1
	4	32.80	2.60	0.288	0.020	0.46	3.472	0.241	0.862	0.057	0.25	1631.5	113.3	3574.6	283.4	5027.8	332.5	-56.4	136.0
	5	37.20	1.90	0.327	0.013	0.27	3.058	0.122	0.831	0.042	0.45	1823.8	72.5	3698.9	188.9	4975.8	251.5	18.6	113.7
	6	43.40	2.50	0.349	0.014	0.44	2.865	0.115	0.909	0.048	0.27	1929.8	77.4	3851.6	221.9	5102.9	269.5	-204.0	142.2
	7	98.90	3.70	0.806	0.025	0.58	1.241	0.038	0.894	0.03	0.29	3810.6	118.2	4675.0	174.9	5079.4	170.5	-375.2	214.7
	8	48.50	2.80	0.412	0.015	0.20	2.427	0.088	0.849	0.051	0.42	2224.1	81.0	3962.0	228.7	5006.2	300.7	-37.0	174.1
	9	30.30	1.80	0.241	0.008	0.22	4.151	0.143	0.902	0.054	0.41	1391.4	47.9	3496.6	207.7	5092.0	304.8	-126.4	109.0
	10	90.80	3.70	0.776	0.022	0.39	1.289	0.036	0.868	0.033	0.32	3702.6	105.0	4589.1	187.0	5037.6	191.5	-191.5	220.2
	11	41.90	2.00	0.350	0.012	0.03	2.857	0.098	0.867	0.046	0.56	1934.6	66.3	3816.7	182.2	5036.0	267.2	-83.0	134.6

ρ refers to an error correlation algorithm that employs the uncertainties on the U-Pb isotopic data uncorrected for common Pb,
where $\rho = [(err^{207}Pb/^{235}U)^2 + (err^{206}Pb/^{238}U)^2 - (err^{207}Pb/^{206}Pb)^2] \div [2 \times (err^{207}Pb/^{235}U) \times (err^{206}Pb/^{238}U)]$ *refers to* $^{206}Pb/^{238}U$ *common Pb-corrected age.*

5. DISCUSSION

REE behaviour

Chondrite (C1)-normalized REE patterns of apatite crystals mimic those of the parent granitoid samples. The apatite-rich cumulates lack any other REE carriers, as apatite is the main REE-bearing mineral phase in these rocks. Hence only apatite and feldspar (both plagioclase and K-feldspar) compete for the REE, in which is similar to the REE behaviour of mafic magmatic systems (Hoskin *et al.*, 2000; Chu *et al.*, 2009). This is in agreement with the inferred origin of the apatite-rich cumulates as being linked to the mantle-related hybrid melts (Szopa *et al.*, 2013).

Both the Goryczkowa and High Tatra granites show the fractionated REE patterns, with HREE depletion and almost lacking Eu anomaly.

In the High Tatra granite, apatite with depleted LREE patterns coexists with monazite and xenotime. As monazite strongly favours LREE and its REE partition coefficients are typically at a maximum at Nd, this could produce Sm and Gd enrichment in co-existing apatite (Yurimoto *et al.*, 1990; Prowatke and Klemme, 2006; Chu *et al.*, 2009). Xenotime is a common carrier phase for Y and HREE. Two types of LREE patterns observed in apatite from the High Tatra granitoids, mirror two genetic magma types that contribute to this layered magma series (Gawęda, 2009; Gawęda and Szopa, 2011). Strong Sm enrichment and simultaneous impoverishment in Y in HTG-A could be related to monazite- and xenotime-related apatite, while relatively flat LREE in HTG-B (**Fig. 3a**; **Table 1**) could be interpreted in terms of a mafic magma influence, with apatite governing the LREE and HREE behaviour, similarly to apatite-rich cumulates from the Western Tatra Mountains (compare **Fig. 3a** and **3c**).

In case of the Goryczkowa variety the presence of allanite and titanite (Burda *et al.*, 2013b) likely cause the depletion in LREE in apatite. Depletion in LREE has been reported in apatites from strongly fractionated granites and pegmatites (Belousova *et al.*, 2002) and was interpreted as a result of the competition with LREE-bearing minerals. Both the Goryczkowa and High Tatra granitoids represent rather weakly fractionated melts, influenced by mixing with mafic magmas, but the competition with LREE-carrier phases has strongly influenced the apatite REE patterns.

The strong negative Eu anomaly is a typical feature of all analysed apatites and could reflect both feldspar crystallization prior to or simultaneously with apatite crystallization and/or the redox state of the host magma (Bea, 1996). This conclusion is supported by the REE K-feldspar patterns, that exhibit strongly positive Eu anomalies (Gawęda and Sikorska, 2009; **Fig. 3a**).

Significance of the apatite U-Pb ages

The U-Pb system in apatite is characterised by a relatively low closure temperature (350–550°C) and as a consequence the system can be easily reset during heating. As apatite crystal size is an important factor for Pb volume diffusion, large apatite grains were analysed where possible. In case of the three analysed samples the calculated LA-ICP-MS U-Pb apatite age is almost identical (within uncertainties) with a mean value of 340 Ma. The c. 340 Ma age is comparable with the youngest U-Pb zircon age of granitoid magmatism in the High Tatra Mountains (337 ± 6 Ma; Burda *et al.*, 2013a). A possible explanation for this is that the U-Pb system in apatite crystals was subsequently disturbed in the whole massif, as a result of the influx of the youngest mantle-related granitoid magma.

The similarity of the youngest LA-ICP-MS U-Pb concordia zircon age and the LA-ICP-MS U-Pb lower intercept apatite ages most likely suggests that cooling occurred in a relatively short time after the last magmatic episode and that no younger thermal events (above 350°C) have occurred in the Tatra Mountains.

ACKNOWLEDGEMENTS

The National Center of Sciences (Poland) sponsored the investigations, by grants 2012/07/B/ST10/04366 (given to AG) and 2011/01/N/ST10/07098 (given to KS). Authors greatly acknowledge the referees (Monika Kusiak and Urs Klötzli) for the valuable comments, important for the present form of the paper.

REFERENCES

Bea F, 1996. Residence of REE, Y, Th and U in granites and crustal protoliths; implications for the chemistry of crustal melts. *Journal of Petrology* 37(3) 521–552, DOI 10.1093/petrology/37.3.521.

Belousova EA, Griffin WL, O`Reilly SY and Fisher NI, 2002. Apatite as an indicator mineral for mineral exploration: trace element compositions and their relationship to host rocks type. *Journal of Geochemical Exploration* 76(1): 45–69, DOI 10.1016/S0375-6742(02)00204-2.

Broska I and Uher P, 2001. Whole-rock chemistry and genetic typology of the West-Carpathian Variscan granites. *Geologia Carpathica* 52: 79–90.

Burda J and Gawęda A, 2009. Shear-influenced partial melting in the Western Tatra metamorphic complex: geochemistry and geochronology. *Lithos* 110(1–4): 373–385, DOI 10.1016/j.lithos.2009.01.010.

Burda J, Gawęda A and Klötzli U, 2011. Magma hybridization in the Western Tatra Mountains granitoid intrusion (S-Poland, Western Carpathians). *Mineralogy and Petrology* 103(1–4): 19–36, DOI 10.1007/s00710-011-0150-1.

Burda J, Gawęda A and Klötzli U, 2013a. U-Pb zircon age of the youngest magmatic activity in the High Tatra granite. *Geochronometria* 40(2): 134–144, DOI 10.2478/s13386-013-0106-9.

Burda J, Gawęda A and Klötzli U, 2013b. Geochronology and petrogenesis of granitoid rocks from the Goryczkowa Unit, Tatra Mountains (Central Western Carpathians). *Geologica Carpathica* 64(6): 419–435, DOI 10.2478/geoca-2013-0029.

Chamberlain KR and Bowring SA, 2000. Apatite-feldspar U-Pb thermochronometer: A reliable, mid-range (450°C), diffusion con-

trolled system. *Chemical Geology* 172(1–2): 173–200, DOI 10.1016/S0009-2541(00)00242-4.

Chew DM, Sylvester PJ and Tubrett MN, 2011. U-Pb and Th-Pb dating of apatite by LA-ICP-MS. *Chemical Geology* 280(1–2): 200–216, DOI 10.1016/j.chemgeo.2010.11.010.

Chew DM and Donelick RA, 2012. Combined apatite fission track and U-Pb dating by LA-ICPMS and future trends in apatite provenance analysis. In: Sylvester, P. Ed., *Quantitative Mineralogy and Microanalysis of Sediments and Sedimentary Rocks*. Mineralogical Association of Canada: 219–248.

Chew DM, Petrus JA and Kamber BS, 2014. U-Pb LA-ICPMS dating using accessory mineral standards with variable common Pb. *Chemical Geology* 363: 185–199, DOI 10.1016/j.chemgeo.2013.11.006.

Chu M, Wang K, Griffin W, Chung S, O`Reilly S, Pearson N and Iizuka I, 2009. Apatite composition: tracing petrogenetic processes in Transhimalayan granitoids. *Journal of Petrology* 50(10): 1829–1855, DOI 10.1093/petrology/egp054.

Cochrane R, Spikings RA, Chew D, Wotzlaw J-F, Chiaradia M, Tyrrell S, Schaltegger U and Van der Lelij R, 2014. High temperature (> 350°C) thermochronology and mechanisms of Pb loss in apatite. *Geochimica et Cosmochimica Acta* 127: 39–56, DOI 10.1016/j.gca.2013.11.028.

Dempster TJ, Jolivet M, Tubrett MN and Braithwaite CJR, 2003. Magmatic zoning in apatite: a monitor of porosity and permeability change in granites. *Contribution to Mineralogy and Petrology* 145: 568–577, DOI 10.1007/s00410-003-0471-0.

Gawęda A, 2008. Apatite-rich enclave in the High Tatra granite, Western Carpathians: petrological and geochronological study. *Geologica Carpathica* 59(4): 295–306.

Gawęda A, 2009. Enclaves in the High Tatra Granite. *University of Silesia publishing House, Monographic series 2637*, Katowice: 180 pages (in Polish, English abstract).

Gawęda A, Doniecki T, Burda J and Kohút M, 2005. The petrogenesis of quartz-diorites from the Tatra Mountains (Central Western Carpathians): an example of magma hybridisation. *Neues Jahrbuch für Mineralogie Abhandlungen* 181(1): 95–109.

Gawęda A and Sikorska M, 2009. Alkali feldspar megacrysts from the High Tatra granite – indicators of magma mixing/mingling processes. *Mineralogia – Special Papers* 35: 82.

Gawęda A and Szopa K, 2011. The origin of magmatic layering in the High Tatra granite, Central Western Carpathians – implications for the formation of granitoid plutons. *Earth and Environmental Science Transactions of the Royal Society of Edinburgh* 102(2): 129–144, DOI 10.1017/S1755691012010146.

Hoskin PWO, Kinny PD, Wyborn D and Chappell BW, 2000. Identifying accessory mineral saturation during differentiation in granitoid magmas: an integrated approach. *Journal of Petrology* 41(9): 1365–1396, DOI 10.1093/petrology/41.9.1365.

Kohút M and Janak M, 1994. Granitoids of the Tatra Mts., Western Carpathians: Field relations and petrogenetic implications. *Geologica Carpathica* 45(5): 301–311.

Kohut M and Sherlock S, 2003. Laser microprobe 40Ar–39Ar analysis of pseudotachylyte and host-rocks from the Tatra Mountains, Slovakia: evidence for late Palaeogene seismic/tectonic activity. *Terra Nova* 15(6): 417–424, DOI 10.1046/j.1365-3121.2003.00514.x.

Jurewicz E, 2006. Petrophysical control on the mode of shearing in the sedimentary rocks and granitoid core of the Tatra Mountain during Late Cretaceous nappe thrusting and folding, Carpathians, Poland. *Acta Geologica Polonica* 56(2): 159–170.

Morozewicz K, 1914. Über die Tatragranite. *Neues Jahrbuch für Geologie und Palaontologie-Abhandlungen* 39: 289–345.

Paton C, Helistrom J, Paul B, Woodhead J and Herqt J, 2011. Iolite: freeware for the visualisation and processing of mass spectrometric data. *Journal of Analytical Atomic Spectrometry* 26: 2508–2518, DOI 10.1039/C1JA10172B.

Petrus JA and Kamber BS, 2012. VizualAge: A Novel Approach to Laser Ablation ICP-MS U-Pb Geochronology Data Reduction. *Geostandards and Geoanalytical Research* 36(3): 247–270, DOI 10.1111/j.1751-908X.2012.00158.x.

Piccoli PM and Candela PA, 2002. Apatite in igneous systems. *Review in Mineralogy and Geochemistry* 48(1): 255–292, DOI 10.2138/rmg.2002.48.6.

Poller U and Todt W, 2000. U-Pb single zircon data of granitoids from the High Tatra Mountains (Slovakia): implications for the geodynamic evolution. *Transactions of the Royal Society of Edinburgh: Earth Sciences* 91(1–2): 235–243, DOI 10.1017/S0263593300007409.

Poller U, Janak M, Kohút M. and Todt W, 2000. Early Variscan magmatism in the Western Carpathians: U-Pb zircon data from granitoids and orthogneisses of the Tatra Mountains, Slovakia. *International Journal of Earth Sciences* 89(2): 336–349, DOI 10.1007/s005310000082.

Prowatke S and Klemme S, 2006. Trace element partitioning between apatite and silicate melt. *Geochimica et Cosmochimica Acta* 70(17): 4513–4527, DOI 10.1016/j.gca.2006.06.162.

Schoene B and Bowring SA, 2006. U-Pb systematics of the McClure Mountain syenite: thermochronological constraints on the age of the Ar-40/Ar-39 standard MMhb. *Contributions to Mineralogy and Petrology* 151(5): 615–630, DOI 10.1007/s00410-006-0077-4.

Schoene B and Bowring SA, 2007. Determining accurate temperature-time paths from U-Pb thermochronology: An example from the Kaapval craton, southern Africa. *Geochimica et Cosmochimica Acta* 71(1): 165–185, DOI 10.1016/j.gca.2006.08.029.

Sha L-K and Chappell BW, 1999. Apatite chemical composition, determined by electron microprobe and laser-ablation inductively coupled plasma mass spectrometry, as a probe into granite petrogenesis. *Geochimica et Cosmochimica Acta* 63(22): 3861–3881, DOI 10.1016/S0016-7037(99)00210-0.

Stacey JS and Kramers JD, 1975. Approximation of terrestrial lead isotope evolution by a two stage model. *Earth and Planetary Science Letters* 26(2): 207–221, DOI 10.1016/0012-821X(75)90088-6.

Sun SS and McDonough WF, 1989. Chemical and isotopical systematics of oceanic basalts: implications for mantle composition and processes. *Magmatism in the Oceanic Basins. Geological Society Special Publications* 42: 313–345.

Szopa K, Gawęda A, Müller A and Sikorska M, 2013. The petrogenesis of granitoid rocks unusually rich in apatite in the Western Tatra Mts. (S-Poland, Western Carpathians). *Mineralogy and Petrology* 107(4): 609–627, DOI 10.1007/s00710-012-0262-2.

Yurimoto H, Duke EF, Papike JJ and Shearer CK, 1990. Are discontinuous chondrite-normalized REE patterns in pegmatitic granite systems the results of monazite fractionation? *Geochimica et Cosmochimica Acta* 54(7): 2141–2145, DOI 10.1016/0016-7037(90)90277-R.